

Microscopic analysis of noise and nonlinear dynamics in *p*-type germanium

T. Kuhn

Institut für Theoretische Physik, Universität Stuttgart, Pfaffenwaldring 57, 7000 Stuttgart 80, Germany

G. Hüpper, W. Quade, A. Rein,* and E. Schöll

Institut für Theoretische Physik, Technische Universität Berlin, Hardenbergstrasse 36, 1000 Berlin 12, Germany

L. Varani and L. Reggiani

Dipartimento di Fisica, Università di Modena, Via Campi 213/A, 41100 Modena, Italy

(Received 18 November 1992)

We analyze the impurity breakdown in *p*-type germanium at liquid-helium temperature on a microscopic level. By using a Monte Carlo simulation including capture and impact ionization processes from shallow impurities, the field-dependent trapping and generation rates are calculated. The current noise is investigated within a two-step process: thermal noise is obtained directly from the Monte Carlo simulation and generation-recombination noise is obtained from a two-level model using the calculated transition rates. In the region close to the phase transition between a nonconducting and a conducting state, various scenarios of nonlinear dynamics related to the dynamical Hall effect have been found.

I. INTRODUCTION

At liquid-helium temperature, *p*-type germanium is known to exhibit a transition from a nonconducting to a conducting state at applied fields of a few V/cm. This transition is so sharp that it can be described in terms of a nonequilibrium phase transition. In the transition region, phenomena like critical slowing down of fluctuations of the carrier concentration and scenarios of nonlinear dynamics like intermittency and chaotic behavior have been theoretically predicted and experimentally observed.¹⁻⁴ The physical mechanism at the basis of these phenomena is the impact ionization of shallow traps which, otherwise frozen out because of the low temperature, are ionized as a consequence of the increasing applied electric field.

Up until now, the microscopic description of this problem has been based on more or less approximate solutions of the Boltzmann equation. In particular, the chaotic behavior has been analyzed in some detail with the aid of the balance equation method.⁵ These equations can be regarded as originating from a moment expansion of the Boltzmann equation. However, the phenomenological rates entering this method as necessary input parameters are in general not directly related to the microscopic characteristics of the material.

The aim of this paper is to overcome the drawbacks of the existing theoretical approaches by using a two-step microscopic analysis which combines a Monte Carlo technique for the calculation of the static characteristics and the high-frequency part of the noise with a hydrodynamic approach, which, for the analysis of the nonlinear dynamics and the low-frequency noise, makes use of the rates obtained from the Monte Carlo simulations. In this way we believe that the physics of the problem is more transparent and no arbitrary parameters are asked for to interpret experimental data as well as to predict a

wide range of intermittency and chaotic behavior.

The paper is organized as follows: In Sec. II we begin with a description of the physical model. The set of balance equations is introduced, and the relation between the microscopic probabilities entering the kinetic description and the characteristic rates in the balance equations is given. The features of the Monte Carlo simulator are briefly described. Section III presents the static characteristics which result directly from the simulations: the mean values of carrier concentration, drift velocity, and carrier energy, as well as the corresponding relaxation rate coefficients as functions of the electric field.

In Sec. IV these results are then applied to a study of noise. The total noise is decomposed into two contributions: fluctuations in the number of free carriers and fluctuations in their drift velocity. Due to strongly different time scales, a combined technique is used: the former contribution is calculated from the rate coefficients, while the latter one is directly obtained from the Monte Carlo simulation. We analyze the characteristic lifetime of carrier number fluctuations and the low-frequency value of the noise spectral density. Thus we obtain quantitatively the critical slowing down and the strong increase of fluctuations near the nonequilibrium phase transition. In a certain range of electric fields, the drift-velocity correlation function exhibits an oscillatory behavior related to a streaming motion contribution induced by optical-phonon emission.

In Sec. V we use the results from the Monte Carlo simulations for an analysis of the nonlinear dynamics associated with the dynamical Hall effect. We report the observation of a regime of oscillatory instabilities, chaos, and intermittency of type I. In the intermittency scenario, the mean laminar length of the oscillations as a function of the magnetic field is shown to obey a critical scaling law. We want to emphasize that here these phenomena are not obtained by choosing "by hand" appropriate coefficients, as is normally done, but rather by

using coefficients which are obtained by solving the Boltzmann equation and which therefore are directly related to the microscopic details of the scattering processes.

II. PHYSICAL MODEL

In a balance equations approach, the drift velocity v_d and the mean carrier energy E for the case of a homogeneous p -type system satisfy the relaxation equations

$$\dot{v}_d = \frac{e\mathcal{E}}{m} - \frac{v_d}{\tau_m} \quad (1)$$

and

$$\dot{E} = e\mathcal{E}v_d - \frac{E - \frac{3}{2}k_B T_L}{\tau_E} \quad (2)$$

Here, \mathcal{E} denotes the electric field, T_L the lattice temperature, m the carrier effective mass, and k_B the Boltzmann constant. Thus, under stationary conditions the momentum (τ_m^{-1}) and energy (τ_E^{-1}) relaxation rates can be obtained from the drift velocity and mean energy according to

$$\tau_m^{-1} = \frac{e\mathcal{E}}{mv_d} \quad (3)$$

and

$$\tau_E^{-1} = \frac{e\mathcal{E}v_d}{E - \frac{3}{2}k_B T_L} \quad (4)$$

While at high temperatures in a doped sample practically all dopants are ionized, at low temperatures they are partially neutral and the concentration of free carriers varies with field. Taking into account the processes of thermal generation (with rate X_1^S), trapping (with coefficient T_1^S), and impact ionization (with coefficient X_1), the free carrier concentration (hole concentration) n satisfies the balance equation

$$\dot{n} = X_1^S n_t + X_1 n n_t - T_1^S n p_t, \quad (5)$$

where $p_t = n + n_D$ is the concentration of ionized acceptors and $n_t = n_A - n_D - n$ the concentration of neutral acceptors. Here, n_A is the acceptor concentration and n_D the concentration of the compensating donors. For symmetry reasons, the process inverse to impact ionization, which is Auger recombination, should also be included. Under low doping conditions, however, this process plays a negligible role and therefore it will not be taken into account in this work.

For a detailed understanding, the coefficients appearing in Eq. (5) have to be related to microscopic transition rates. Here we treat the impurity within a one-level model where only the ground state is taken into account. The impact ionization coefficient is given from the microscopic transition rate $P_{ii}(\mathbf{k} \rightarrow \mathbf{k}', \mathbf{k}'')$ for a carrier making a transition from crystal momentum state \mathbf{k} to \mathbf{k}' and generating a new carrier with \mathbf{k}'' according to

$$X_1 = \frac{1}{n n_t} \int d^3k d^3k' d^3k'' f(\mathbf{k}) P_{ii}(\mathbf{k} \rightarrow \mathbf{k}', \mathbf{k}''), \quad (6)$$

where $f(\mathbf{k})$ is the distribution function of the free carriers. The trapping coefficient is given from the microscopic capture rate $P_{\text{trap}}(\mathbf{k})$ of a carrier with momentum \mathbf{k} into the bound state according to

$$T_1^S = \frac{1}{n p_t} \int d^3k f(\mathbf{k}) P_{\text{trap}}(\mathbf{k}), \quad (7)$$

and the thermal generation rate is determined by the transition rate $P_{\text{gen}}(\mathbf{k}')$ from the bound state to a state with momentum \mathbf{k}' according to

$$X_1^S = \int d^3k' P_{\text{gen}}(\mathbf{k}'). \quad (8)$$

In the Monte Carlo simulator we use a single valence band, the heavy-hole band, where warping and nonparabolicity are taken into account. The intraband scattering processes are elastic scattering by ionized impurities treated in Conwell-Weisskopf approximation, as well as inelastic scattering by both acoustic (AP) and optical (OP) phonons due to deformation-potential interaction. Trapping processes from the band to the impurity level are treated within the "cascade capture model."^{6,7} In addition, impact ionization processes, here treated in Keldysh approximation,^{8,9} lead to a transition from the impurity level to the band. For details of the band-impurity transitions, the reader is referred to Ref. 10.

The details of the Monte Carlo simulator are described in Refs. 11 and 12. It is a standard one-particle simulator¹³ based on the ergodicity of the system and consequently can describe only stationary situations. The simulated particle is subjected to successive scattering processes. If it performs an impact ionization process, it is placed arbitrarily on the energy sphere that corresponds to the initial energy minus the trap energy. After a trapping process, it is immediately regenerated with a \mathbf{k} value according to P_{gen} . This procedure is justified under the assumption of a stationary distribution function. The

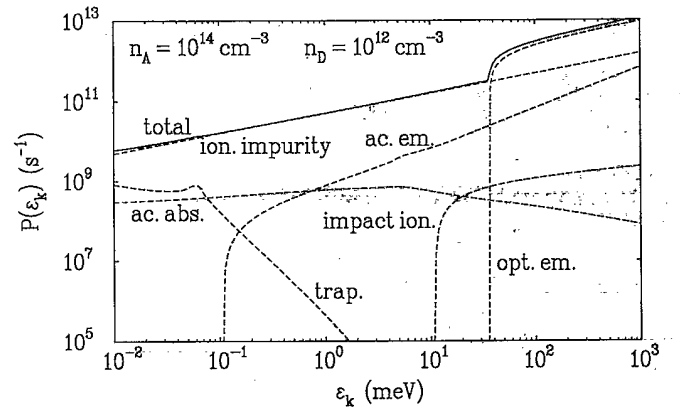


FIG. 1. Microscopic scattering rates as functions of the microscopic carrier energy used in the Monte Carlo simulation: acoustic absorption (ac. abs.); acoustic emission (ac. em.); optical emission (opt. em.); ionized impurity (ion. impurity); impact ionization (impact ion.); trapping (trap.). The rates are calculated for holes in germanium for the given acceptor and donor concentrations at a lattice temperature of 4 K. For material parameters see Table I.

TABLE I. Material parameters for holes in germanium used in the simulations. Due to the nonparabolicity, the effective mass depends on the carrier energy.

Effective mass at $T_h = 4$ K	$0.346m_0$
Effective mass at $T_h = 1000$ K	$0.476m_0$
Crystal density	5.32 g cm^{-3}
Sound velocity	$3.93 \times 10^5 \text{ cm s}^{-1}$
Optical-phonon temperature	430 K
Relative static dielectric constant	16.0
Acoustic deformation potential	4.6 eV
Optical deformation potential	$9.0 \times 10^8 \text{ eV cm}^{-1}$
Equilibrium volume recombination rate	$6.5 \times 10^{-5} \text{ cm}^3 \text{ s}^{-1}$
Equilibrium generation rate	$2.1 \times 10^{-3} \text{ s}^{-1}$
Energy of the acceptor level	11 meV
Cross section for impact ionization	$3.15 \times 10^{-13} \text{ cm}^2$

effects of trapping, generation, and impact ionization on the free carrier dynamics, especially the energy loss and the randomization of carrier momentum, are thus fully taken into account in the simulation.

The macroscopic coefficients are obtained from the simulation according to Eqs. (6) and (7). Since the microscopic transition rates depend on the concentration of ionized and neutral impurities, for the case of a one-particle simulator an iterative procedure is necessary: Given the coefficients, Eq. (5) yields a value for the stationary carrier concentration. This concentration is used as new input value for the Monte Carlo simulation. This procedure is repeated until convergence occurs which requires typically three to five iteration steps.

In Fig. 1 the microscopic rates of all the included scattering processes are shown for an acceptor concentration of $n_A = 10^{14} \text{ cm}^{-3}$ and a donor concentration of $n_D = 10^{12} \text{ cm}^{-3}$. The density-dependent rates are plotted for the case of a vanishing free carrier concentration referring to the lowest value of the electric field. It can be seen that the time scales for intraband scattering processes (in particular, ionized impurity scattering and optical-phonon emission) are much shorter than trapping and impact ionization processes. In this case the shape of the distribution function is mainly determined by intraband processes (see also Table I).

III. STATIC PROPERTIES

Using the Monte Carlo simulation, the dependences of the drift velocity v_d , mean energy E , and concentration of free carriers n on the applied electric field have been determined. The results for two donor concentrations are shown in Fig. 2 where the mean energy is expressed in terms of a hole temperature according to $E = \frac{3}{2} k_B T_h$. For electric fields above 10 V/cm, the values are independent of the donor concentration. Below, however, they are largely influenced. A higher compensation shifts the breakdown associated with the sharp rise in n to higher voltages, in agreement with the simple phenomenological theory.¹ Due to the increased scattering by ionized impurities, the drift velocity is strongly reduced in the region below threshold. This scattering process, although being elastic, also reduces the carrier heating by preventing long free flights where the carriers could gain energy

from the external field.

The drift velocity and mean energy have then been used to determine the relaxation rates for momentum (τ_m^{-1}) and energy (τ_E^{-1}) according to Eqs. (3) and (4). The impact ionization (X_1) and trapping (T_1^S) coefficients have been calculated according to their definitions [Eqs. (6) and (7)]. In Fig. 3 the rates τ_m^{-1} , τ_E^{-1} , $n_A X_1$, and $n_A T_1^S$ are shown as functions of the electric field for the same cases as in Fig. 2. At the lowest fields, the momentum relaxation rate is approximately independent of the field reflecting the Ohmic behavior of the transport. For the lower donor concentration it is increasing monotonically due to the increase in the efficiency of phonon scattering which dominates the decreasing efficiency of impurity scattering. For the higher donor concentration this latter effect dominates in the region just before the breakdown leading to a nonmonotonic behavior. The energy relaxation rate exhibits the well-known behavior:¹⁴ With increasing field it first approaches the momentum relaxation rate and then decreases again at the highest fields due to the reduced efficiency of optical-phonon emission. The trapping coefficient decreases with increasing field since only carriers in states with very small energy can perform trapping processes (see Fig. 1). The occupation

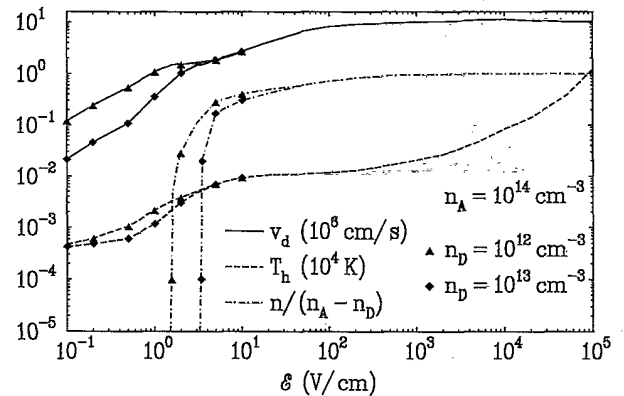


FIG. 2. Mean values of free carrier concentration n , drift velocity v_d , and carrier energy E (expressed in terms of a carrier temperature $E = \frac{3}{2} k_B T_h$) as functions of the electric field for the given acceptor and donor concentrations.

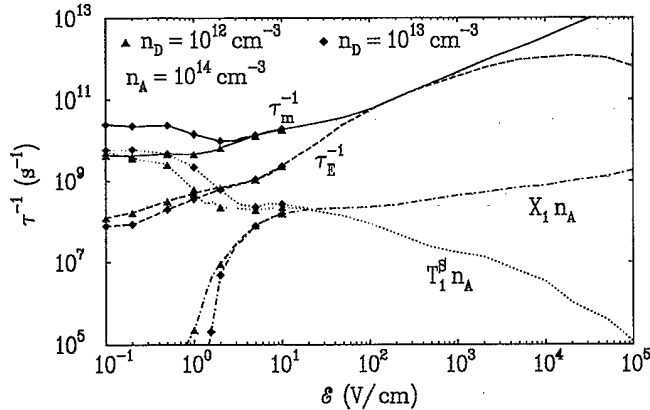


FIG. 3. Momentum (τ_m^{-1}) and energy (τ_E^{-1}) relaxation rates, as well as impact ionization (X_I) and trapping (T_1^β) coefficient, multiplied by the acceptor concentration as functions of the electric field for the given acceptor and donor concentrations.

of these states is strongly reduced with increasing carrier temperature. The impact ionization coefficient, on the other hand, requires an activation energy and therefore is negligible at low fields. It increases strongly at a field of the order of 1 V/cm, leading to the impurity breakdown. This increase is shifted towards higher fields and becomes sharper with increasing donor concentration.

IV. FLUCTUATIONS

After discussing the static characteristics, we now turn to the fluctuations $\delta I(t)$ of the current $I(t)$ and thus to the noise of the system. The experimentally observed noise spectrum is related to the current correlation functions according to the Wiener-Khinchine theorem

$$S_I(f) = 2 \int_{-\infty}^{\infty} \langle \delta I(0) \delta I(t) \rangle e^{2\pi i f t} dt, \quad (9)$$

where $I(t) = \langle I \rangle + \delta I(t)$ is the instantaneous value of the total current and the angle brackets denote a time average. Due to the Ramo-Shockley theorem, in a homogeneous sample of length L under constant voltage condition, it is proportional to the product of the number of carriers N inside the sample and their drift velocity. Thus, the total noise can be decomposed into three different contributions:¹² thermal noise related to fluctuations in the drift velocity, generation-recombination noise related to fluctuations in the number of free carriers, and noise due to cross correlations between both types of fluctuations. In the present case, where the time scales of scattering processes and trapping-detrapping processes are largely different, cross correlations can be neglected¹² and the current correlation function is given by

$$\begin{aligned} \langle \delta I(0) \delta I(t) \rangle &= \frac{e^2}{L^2} \langle N \rangle^2 \langle \delta v_d(0) \delta v_d(t) \rangle \\ &+ \langle v_d \rangle^2 \langle \delta N(0) \delta N(t) \rangle. \end{aligned} \quad (10)$$

Motivated by the difference in the time scales, the two contributions have been calculated by different techniques: The thermal noise is mainly governed by the fast intraband scattering processes; the velocity correlation

function is therefore calculated directly in the Monte Carlo simulation. The generation-recombination noise can be reduced to an effective two-level dynamics with transition coefficients given by Eqs. (6)–(8).

Let us first discuss the velocity correlation function. It is plotted for the longitudinal as well as for the transverse case in Fig. 4. At the lowest field, both correlation functions coincide and exhibit an exponential decay, as expected close to equilibrium. For symmetry reasons the transverse velocity does not couple to other variables; thus, its correlation function always decays exponentially, the decay rate being related to the momentum relaxation rate. With increasing field, due to the onset of hot-carrier conditions, momentum and energy relaxation processes couple in the direction of the field: The correlation function of the longitudinal velocity first decays to a negative value with the momentum relaxation rate and then returns to zero with the energy relaxation rate. A detailed discussion of these phenomena can be found in Ref. 14 where the case of *p*-type silicon at liquid-nitrogen temperature has been analyzed. In the region between 100 and 1000 V/cm, where the energy and momentum relaxation rates practically coincide, this coupling leads to an oscillatory contribution in the correlation function. The

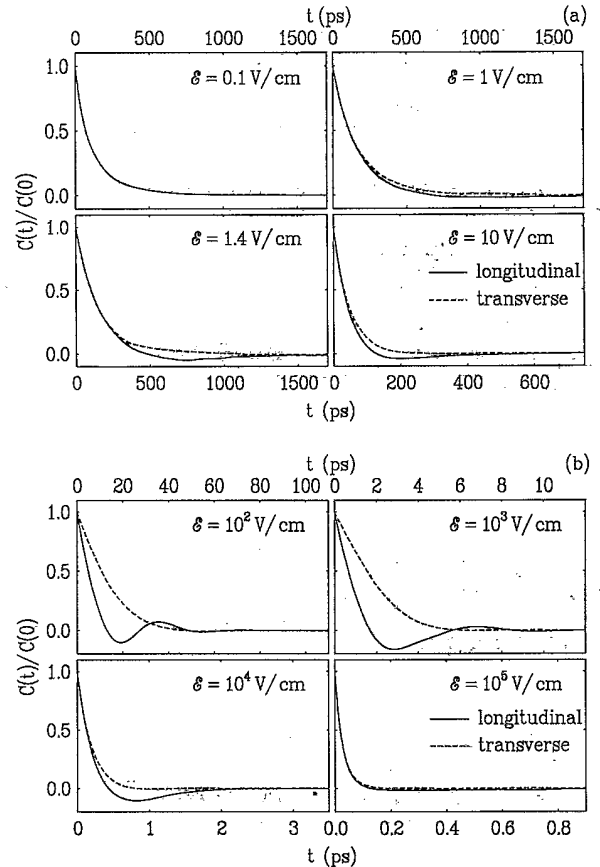


FIG. 4. Normalized correlation functions of velocity fluctuations $C(t) = \langle \delta v_d(0) \delta v_d(t) \rangle$ in longitudinal and transverse direction with respect to the electric field, as a function of time for (a) low and (b) high applied voltages. Calculations refer to the case $n_D = 10^{12} \text{ cm}^{-3}$.

physical origin is a streaming motion character of the transport.^{15,16} The carriers are accelerated up to the threshold of optical-phonon emission, where they emit a phonon returning to the band minimum. This corresponds to a periodic motion in k space, which is damped by other scattering mechanisms and the finite value of the phonon emission rate. In contrast to the case of Si at 77 K, where this damping has been found to prevent a direct observation of oscillations,¹⁴ here they are clearly visible. For further increasing field, energy and momentum relaxation rates again become different, leading to a reduction in the coupling and consequently in the negative part of the correlation function.

The correlation function of velocity fluctuations is responsible for the high-frequency behavior of the noise spectrum. Let us now turn to the low-frequency part governed by carrier number fluctuations. Starting from a master-equation analysis of the effective two-level system consisting of the impurity level and the band, the correlation function of number fluctuations can be expressed in terms of the macroscopic coefficients.¹⁷ One obtains an exponentially decaying correlation function.

$$\langle \delta N(0)\delta N(t) \rangle = \langle \delta N^2 \rangle e^{-t/\tau_l}, \quad (11)$$

and a corresponding Lorentzian noise spectrum,

$$S_I(f) = 4\langle I \rangle^2 \frac{\tau_l}{1 + (2\pi f \tau_l)^2}. \quad (12)$$

The variance is given by

$$\langle \delta N^2 \rangle = V(n_A - n_D) \frac{u(\delta + u)(1 - u)}{1 + \delta - (1 + \gamma)(1 - u)^2} \quad (13)$$

and the inverse lifetime by

$$\tau_l^{-1} = T_1^S \frac{n_A - n_D}{1 - u} [1 + \delta - (1 + \gamma)(1 - u)^2], \quad (14)$$

where V is the volume of the sample and the following abbreviations have been used: $u = n/(n_A - n_D)$, $\delta = n_D/(n_A - n_D)$, and $\gamma = X_1/T_1^S$.

Figure 5 shows the inverse lifetime according to Eq. (14) as a function of the electric field. Close to the breakdown transition, we observe a reduction by about two orders of magnitude, the "critical slowing down" associated with a phase transition. For comparison, the momentum relaxation rate related to velocity fluctuations has also been included. In the whole range there are at least about two orders of magnitude difference, justifying the separate treatment of both contributions to the current noise.

In Fig. 6 the contributions to the low-frequency value of the noise spectrum have been plotted as functions of the electric field. In order to eliminate the geometry parameters, the spectral density $S_I(f)$ has been scaled according to

$$S_I(f) = \frac{4ne^2V}{L^2} s(f) = \frac{4ne^2A}{L} [s_v(f) + s_{gr}(f)], \quad (15)$$

where s_v and s_{gr} refer to velocity and number fluctuations, respectively, and A is the cross section of the sam-

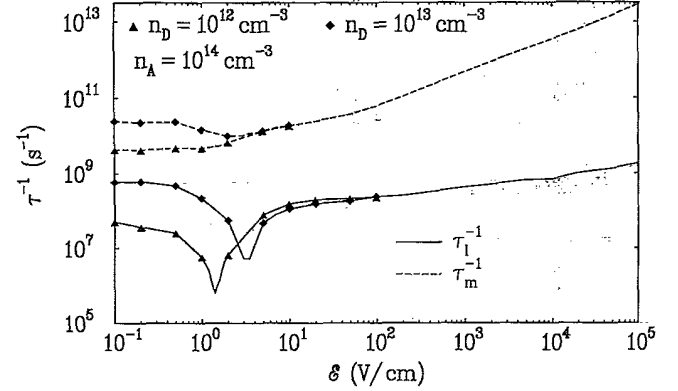


FIG. 5. Inverse lifetime τ_l^{-1} of carrier number fluctuations as a function of the electric field for the given acceptor and donor concentrations. The momentum relaxation rate τ_m^{-1} is also plotted to emphasize the difference in the time scales relevant for velocity and number fluctuations. The minima of τ_l^{-1} evidence the "critical slowing down" of number fluctuations associated with a phase transition.

ple. Except for very low and very high fields, generation-recombination noise is always the dominant contribution. This holds even for fields where more than 99% of the acceptors are already ionized, as has been verified experimentally for the case of p -type Si at 77 K.¹⁸ The main reason is the much larger value of the lifetime compared to the momentum relaxation time. Close to the transition, s_{gr} increases by several orders of magnitude, as expected for a phase transition and observed experimentally.² The overall behavior of the velocity contribution can be understood as a competition between different features: The increasing carrier temperature leads to an increase in $s_v(0)$, while the increase of the momentum relaxation rate leads to a decrease in the noise, both effects dominating in different field ranges.

Finally, in Fig. 7 noise spectra for different values of the electric field are shown as functions of the frequency. They have been obtained by Fourier transformation of

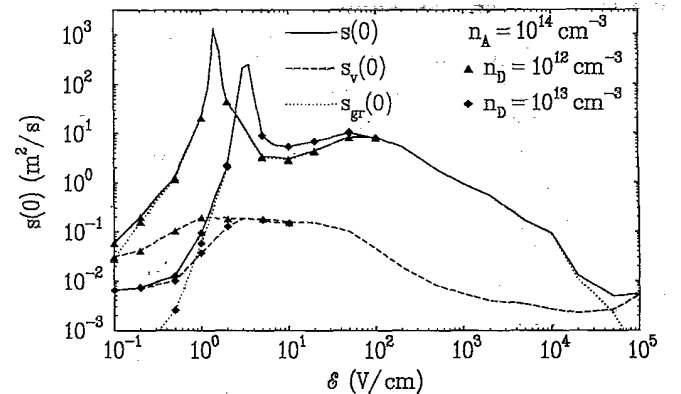


FIG. 6. Low-frequency value of the scaled noise spectral density [see Eq. (15)], as well as the contributions due to velocity and number fluctuations, as functions of the electric field for the given acceptor and donor concentrations.

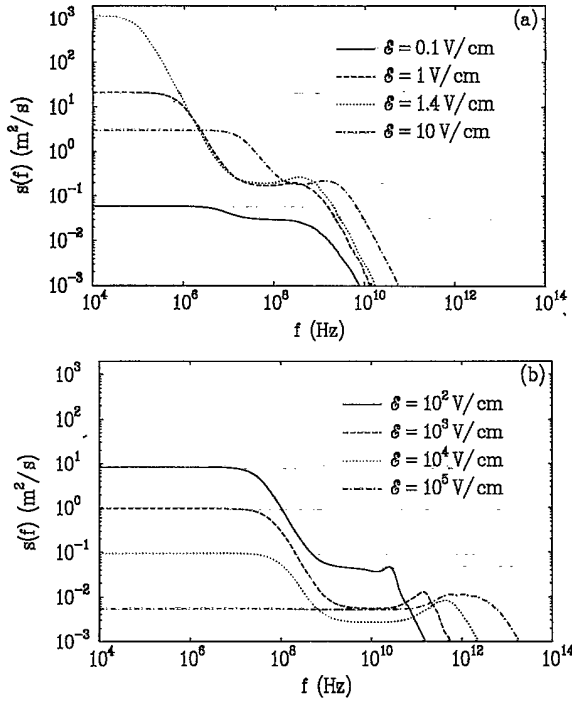


FIG. 7. Scaled noise spectra as functions of frequency at (a) low and (b) high applied fields. Calculations refer to the case $n_D = 10^{12} \text{ cm}^{-3}$.

the velocity correlation function and addition of the Lorentzian due to generation-recombination noise. The coupling between energy and momentum relaxation results in a nonmonotonic behavior of the noise spectra: A local maximum is appearing beyond the cutoff frequency of generation-recombination noise. For an oscillating correlation function this maximum is above the line of the asymptotic high-frequency decay; if there is only a negative part in the correlation function, it is below this.¹⁹

V. INTERMITTENCY AND CHAOS

Besides critical slowing down and increase of noise, the nonequilibrium phase transition from a nonconducting to a conducting state induced by impact ionization of acceptors is associated with various scenarios of nonlinear dynamics. While the investigation of the fluctuations is performed with fixed electric field (*voltage control*), where the system is stable against fluctuations, the dynamic behavior of the system changes significantly under *current control*. In this area a novel mechanism that explains self-generated voltage or current oscillations induced by a transverse magnetic field on the basis of a dynamic Hall effect was proposed recently.²⁰ The main objective of this previous theoretical treatment was the physical origin of these oscillations without using a detailed semiconductor model.

In the framework of balance equations, the system is described by the following three dynamical variables: carrier density n , longitudinal drift field \mathcal{E}_x , and transverse Hall field \mathcal{E}_z . Equation (5) determining the dynamical

behavior of the carrier density is supplemented by the equations of motion for the two components of the field:

$$\epsilon \dot{\mathcal{E}}_x = J_0 - e\mu_B n (\mathcal{E}_x - \mathcal{E}_z \mu \mathcal{B}), \quad (16)$$

$$\epsilon \dot{\mathcal{E}}_z = -e\mu_B n (\mathcal{E}_z + \mathcal{E}_x \mu \mathcal{B}), \quad (17)$$

where ϵ is the permittivity, μ the mobility, $\mu_B = \mu / [1 + (\mu \mathcal{B})^2]$, \mathcal{B} the magnetic induction, and J_0 the externally applied current density. Here we attempt to understand these phenomena on a more microscopic level of description. For the numerical analysis of the dynamics of the system, the field dependence of the transport coefficients appearing in the above equations have been expressed in terms of smooth functions of the field $\mathcal{E} = (\mathcal{E}_x^2 + \mathcal{E}_z^2)^{1/2}$ according to

$$\mu(\mathcal{E}) = \mu_0 (\mathcal{E}_0 + \mathcal{E} / \mathcal{E}_1)^{\alpha_1} \quad (18)$$

for the mobility,

$$X_1(\mathcal{E}) = X_0 \exp[\alpha_2 (\mathcal{E} / \mathcal{E}_1)^{\alpha_3}] \quad (19)$$

for the impact ionization coefficient, and

$$T_1^S(\mathcal{E}) = T_0^S \exp[\alpha_4 (\alpha_5 - \mathcal{E} / \mathcal{E}_1)^2] + \alpha_6 (\alpha_7 - \mathcal{E} / \mathcal{E}_1)^{\alpha_8} \quad (20)$$

for the trapping coefficient. These functions are fitted to our Monte Carlo data. The fit parameters $\alpha_i, \mu_0, X_0, T_0^S$ have been obtained by a nonlinear-regression analysis. They are

$$\begin{aligned} \mu_0 &= 1.3 \times 10^6 \text{ cm}^2 / (\text{V s}), \quad \mathcal{E}_0 = 1.04, \\ \alpha_1 &= -0.64, \quad X_0 = 2.34 \times 10^{-7} \text{ cm}^3 \text{ s}^{-1}, \\ \alpha_2 &= 9.2, \quad \alpha_3 = -1.37, \\ T_0^S &= 5.6 \times 10^{-6} \text{ cm}^3 \text{ s}^{-1}, \quad \alpha_4 = 1.355, \\ \alpha_5 &= 0.76, \quad \alpha_6 = 0.72 \text{ cm}^3 \text{ s}^{-1}, \quad \alpha_7 = 157, \\ \alpha_8 &= -2.05, \quad \mathcal{E}_1 = 1 \text{ V/cm}. \end{aligned}$$

The resulting curves together with the simulation data are shown in Fig. 8. The fits are performed without magnetic field. However, since it turns out that in the relevant field regime, the Hall coefficient is close to unity,²¹ the above expressions can be used for $\mathcal{B} \neq 0$ if substituting the electric field \mathcal{E} by $\mathcal{E}(1 + \mu^2 \mathcal{B}^2)^{-1/2}$.

A linear-stability analysis of the above equations yields necessary but not sufficient conditions for the onset of an oscillatory instability:^{20,21}

$$\frac{1}{\tau_1} < \frac{(\mu \mathcal{B})^2 - 1}{\tau_M^*}, \quad \mu \mathcal{B} > 1 \quad (21)$$

which requires a minimum value of \mathcal{B} and a lifetime which is large compared to the effective dielectric relaxation time

$$\tau_M^* = \epsilon(1 + \mu^2 \mathcal{B}^2) / (en^* \mu_{\text{diff}}),$$

$\mu_{\text{diff}} = dv_d / d\mathcal{E}_x$ being the differential mobility and n^* the steady-state carrier density.

These conditions are fulfilled for the Monte Carlo data

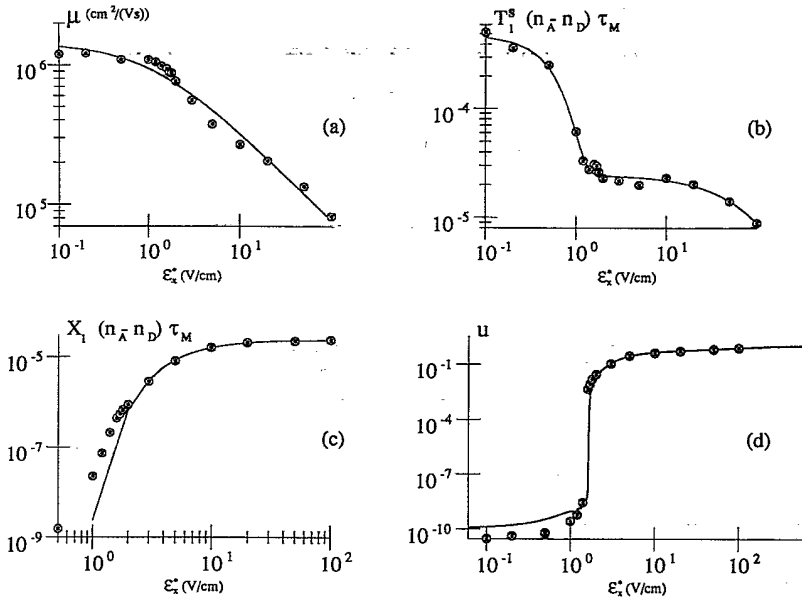


FIG. 8. Transport coefficients obtained from the Monte Carlo simulation together with the analytical fit functions used in the analysis of the nonlinear dynamics: (a) mobility, (b) dimensionless capture coefficient, (c) dimensionless impact ionization coefficient, (d) normalized steady-state carrier density $u = n^*/(n_A - n_D)$ as functions of the steady-state drift field E_x^* . Calculations refer to the case $n_D = 10^{12} \text{ cm}^{-3}$ and $\tau_M = 10^{-13} \text{ s}$.

at the onset of the breakdown where, due to the critical slowing down, the lifetime becomes large, and we obtain—without any adjustable parameter—a regime of oscillatory instabilities in the (E_x^*, \mathcal{B}) plane [Fig. 9(a)], where E_x^* is the steady-state electric field at a certain J_0 and \mathcal{B} .

A numerical integration of the full nonlinear equations (5), (16), and (17) yields the following scenario for the maximum of the density n_{max} as a function of the magnetic field [see Fig. 9(b)]: a Hopf bifurcation of a limit cycle, a period-doubling route to chaos, and type-I intermittency at the end of a period-three window.²² A similar bifurcation diagram is obtained by variation of J_0 .

Figure 10(a) shows an intermittent time series: an almost periodic oscillation is interrupted by chaotic bursts. For fixed magnetic field \mathcal{B} , the length of the laminar periodic oscillations shows a distribution, which is characteristic for type-I intermittency [Fig. 10(b)]. While this characteristic shape of the function remains, the position of the second peak varies as a function of \mathcal{B} . Thus, the main laminar length of the oscillations as a function of the magnetic field obeys a universal scaling behavior $\langle l \rangle \propto (\mathcal{B} - \mathcal{B}_c)^{-1/2}$, \mathcal{B}_c being the critical bifurcation point where the period-three motion ceases, in good agreement with experiments.²³ The scaling property of

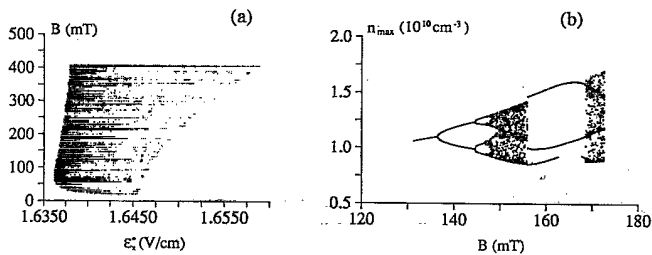


FIG. 9. (a) Phase diagram of the control parameter plane. The dashed area indicates the regime of oscillatory instability. (b) Bifurcation diagram of the maxima of the carrier density vs the control parameter \mathcal{B} for $E_x^* = 1.647 \text{ V/cm}$.

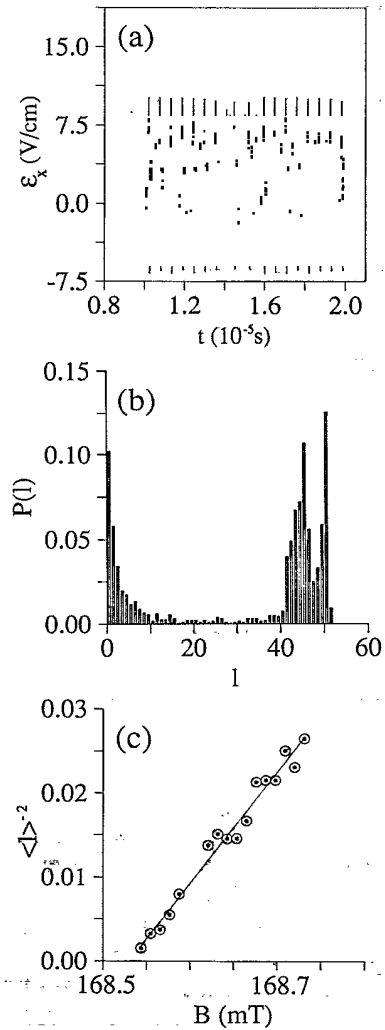


FIG. 10. Type-I intermittency: (a) time series $E_x(t)$, (b) distribution of laminar lengths l for $\mathcal{B} = 168.56 \text{ mT}$, (c) scaling behavior of the mean laminar length $\langle l \rangle$ as a function of the magnetic field for the parameters as in Fig. 9. (The laminar length is given by the number of iterates of the Poincaré map.)

the higher moments of the laminar length which was found recently²⁴ is also verified.²²

VI. CONCLUSIONS

We have presented a detailed microscopic analysis of transport phenomena in *p*-type Ge at liquid-helium temperature. From Monte Carlo simulations the static properties and the resulting phenomenological rates have been obtained. The different time scales of intraband scattering processes and trapping-detrapping processes have enabled us to separate thermal noise related to velocity fluctuations from generation-recombination noise related to fluctuations in the carrier number. The former has been calculated directly within the Monte Carlo simulation, while for the latter, analytical expressions involving the phenomenological rates have been used.

We have found a field region where a strong streaming motion leads to an oscillatory contribution in the velocity correlation function as a function of time. The lifetime of

carrier number fluctuations reflects the critical slowing down close to the phase transition, and the low-frequency value of the noise spectrum is strongly peaked in this region.

The phenomenological rates have then been used for an analysis of the nonlinear dynamics related to the non-equilibrium phase transition. Various scenarios have been found, including oscillatory instabilities, period-doubling routes to chaos, and intermittency of type I. In the latter case, the mean laminar length obeys a universal scaling behavior. Thus, previous results based on simplified models have been confirmed by a realistic modeling of carrier transport in germanium.

ACKNOWLEDGMENTS

We acknowledge partial financial support from the Deutsche Forschungsgemeinschaft (Bonn, Germany) and the Ministero dell'Università e della Ricerca Scientifica (Rome, Italy).

*Present address: Walter-Schottky-Institut, James-Franck-Str., 8046 Garching, Germany.

¹E. Schöll, *Nonequilibrium Phase Transitions in Semiconductors* (Springer, Berlin, 1987).

²M. Pilkuhn, *Z. Naturforsch. Teil A* **16**, 173 (1961); **16**, 182 (1961).

³J. Parisi, U. Rau, J. Peinka, and K. M. Mayer, *Z. Phys. B* **72**, 225 (1988).

⁴W. Clauss, U. Rau, J. Parisi, J. Peinke, R. P. Hübener, H. Leier, and A. Forchel, *J. Appl. Phys.* **67**, 2980 (1990).

⁵E. Schöll, in *Handbook on Semiconductors*, 2nd ed., edited by P. T. Landsberg (North-Holland, Amsterdam, 1992), Vol. 1, Chap. 8.

⁶M. Lax, *Phys. Rev.* **119**, 1502 (1960).

⁷V. N. Abakumov, V. I. Perel, and I. N. Yassievich, *Fiz. Tekh. Poluprovodn.* **12**, 3 (1978) [*Sov. Phys. Semicond.* **12**, 1 (1978)].

⁸L. V. Keldysh, *Zh. Eksp. Teor. Fiz.* **37**, 713 (1960) [*Sov. Phys. JETP* **10**, 509 (1960)].

⁹H. W. Dravin, *Z. Phys.* **164**, 513 (1961).

¹⁰L. Reggiani and V. Mitin, *Riv. Nuovo Cimento* **12**, 1 (1989).

¹¹L. Reggiani, P. Lugli, and V. Mitin, *Appl. Phys. Lett.* **51**, 925 (1987).

¹²T. Kuhn, L. Reggiani, L. Varani, and V. Mittin, *Phys. Rev. B* **42**, 5702 (1990).

¹³C. Jacoboni and L. Reggiani, *Rev. Mod. Phys.* **55**, 645 (1983).

¹⁴T. Kuhn, L. Reggiani, and L. Varani, *Phys. Rev. B* **42**, 11 133 (1990).

¹⁵V. Bareikis, A. Galdikas, R. Miliušyte, and V. Viktoravičius, in *Proceedings of the Sixth International Conference on Noise in Physical Systems, Gaithersburg, Maryland, 1981*, edited by P. H. E. Meijer, R. D. Mountain, and R. J. Soulen, Jr. (National Bureau of Standards, Washington, D.C., 1981), p. 406.

¹⁶V. V. Mitin and C. M. van Vliet, in *Proceedings of the Tenth International Conference on Noise in Physical Systems, Budapest, 1989*, edited by A. Ambrózy (Akadémiai Kiadó, Budapest, 1990), p. 103.

¹⁷K. M. van Vliet and J. R. Fassett, in *Fluctuation Phenomena in Solids*, edited by R. E. Burgess (Academic, New York, 1965).

¹⁸T. Kuhn, L. Reggiani, L. Varani, D. Gasquet, J. C. Vaissière, and J. P. Nougier, *Phys. Rev. B* **44**, 1074 (1991).

¹⁹T. Kuhn, L. Reggiani, and L. Varani, *J. Appl. Phys.* **69**, 7097 (1991).

²⁰G. Hüpper and E. Schöll, *Phys. Rev. Lett.* **66**, 2463 (1991).

²¹G. Hüpper, E. Schöll, and A. Rein, *Mod. Phys. Lett. B* **6**, 1001 (1992).

²²G. Hüpper, W. Quade, A. Rein, E. Schöll, T. Kuhn, L. Reggiani, and L. Varani, in *Proceedings of the Twenty-First Conference on the Physics of Semiconductors, Beijing*, edited by Xie Xide and Kun Huang (World Scientific, Singapore, in press).

²³R. Richter, U. Rau, A. Kittel, G. Heinz, J. Peinke, J. Parisi, and R. P. Huebener, *Z. Naturforsch. Teil A* **46**, 1012 (1992).

²⁴A. Rein, E. Schöll, and G. Hüpper, *Europhys. Lett.* **21**, 7 (1993).